Simulation of chemical erosion in rough fractures

R. Verberg and A. J. C. Ladd*
Chemical Engineering Department, University of Florida, Gainesville, Florida 32611-6005
(Received 20 December 2001; published 17 May 2002)

We report on numerical simulations of acid erosion in a fractured specimen of Carrara marble. The simulations combine two recent advances in lattice-Boltzmann methodology to accurately and efficiently calculate the velocity field in the pore space. A tracer diffusion algorithm was then used to calculate the distribution of reactants in the fracture, and the local erosion rate was obtained from the flux of tracer particles across the surfaces. Our results show that at large length scales, erosion leads to increased heterogeneity via channel formation, whereas at small length scales it tends to smooth out the roughness in the local aperture.

DOI: 10.1103/PhysRevE.65.056311 PACS number(s): 47.11.+j, 47.55.Mh, 47.70.Fw, 92.40.Gc

I. INTRODUCTION

The permeability of rocks is often dominated by flow through fractures, even when the fracture porosity is only a small fraction of the total pore volume. Since the permeability of a fracture scales as the square of the aperture, relative modest erosion of fracture surfaces can cause a significant increase in the overall permeability. On the other hand, erosion of support points can undermine the ability of these points to withstand compressive stresses, leading to fracture collapse and a large reduction in permeability. Recent experiments [1] have shown that acid erosion of narrow fractures can lead to qualitatively different dissolution patterns at large and small length scales, as a result of the complex interplay of transport, chemical kinetics, and surface morphology. At large length scales erosion leads to increased heterogeneity, whereas at small length scales it tends to smooth out fluctuations in the local aperture. Increasing heterogeneity is probably driven by a fingering instability [2,3], in which regions of high porosity erode faster as a result of more rapid replenishment of reactants, as shown with recent experiments in a synthetic two-dimensional porous medium [4]. Similar ''positive feedback loops'' occur in the dissolution of limestone formations (see Refs. [5,6], and references therein). On the other hand, in narrow channels the concentration gradients in the diffusive boundary layer can be larger, causing an increased flow of reactants to the fracture surfaces, as a result small scale roughness is smoothed out. Additional complications can arise from erosion of contact points, resulting in the collapse of parts of the fracture. Fracture collapse can lead to the formation of new pathways and a widening of the remaining channels. Thus, the morphology of the eroded surface is sensitive to the details of the dissolution of contact points.

A fundamental understanding of the role of fractures, and the effects they have on fluid flow, solute transport, and mechanical properties, is an essential component of theoretical models of geological systems. For example, CO_2 sequestration will require predictive models for the effects of fracture on the overall permeability of rock-fluid systems, and more importantly, how this fracture permeability evolves with time [7]. Numerical simulations of dissolution can isolate the effects of different erosion mechanisms in well-defined and repeatable experiments. Furthermore, they offer detailed information on the flow field, the distribution of reactants and products, and the variation in erosion rate throughout the fracture.

A numerical model describing dissolution and precipitation in an evolving fracture aperture was presented by Békri *et al.* [8]. They used a multigrid method to solve for the fluid velocity field, and a finite-difference scheme to calculate the local dissolution or deposition rate at the fracture surfaces. However, the computational demands of the method limited the simulations to a small number of grid points, insufficient for the present study. Also, they did not attempt to account for the effect of confining pressure on the evolution of the surface morphology. Dijk and Berkowitz [9] analyzed dissolution and precipitation in an evolving fracture aperture using a combination of analytical and numerical techniques. They considered fractures with an initially flat or sinusoidal aperture and found that the initial fracture geometry has a profound effect on the reaction process. However, although their results are significant as a basis for more complex models of transport and dissolution in fractured media they did not study a realistic, arbitrarily complex, fracture geometry.

In this paper we describe algorithms to simulate chemical erosion in porous rocks and report preliminary results for acid erosion in a fractured specimen of Carrara marble. The simulation consists of three separate calculations that are iterated to determine the time evolution of the velocity field and surface morphology. From the initial fracture topography, the velocity field is calculated by means of a recently developed lattice-Boltzmann model that allows for a continuous variation in the position of the solid surfaces [10,11]. Next, the steady-state distribution of reactants and the flux of reactants across each fracture surface are determined by a stochastic solution of the convection-diffusion equation in the presence of this velocity field. Finally, a new structure is evolved by eroding material from each fracture surface; the amount of the material is proportional to the local flux of tracer particles across that surface.

In these preliminary calculations it has been assumed that the chemical reaction at the surface is instantaneous and that the rate constant is unaffected by the concentration of reactants or products. This approximation is a model for transport

*URL: http://www.che.ufl.edu/~ladd/Ladd.htm

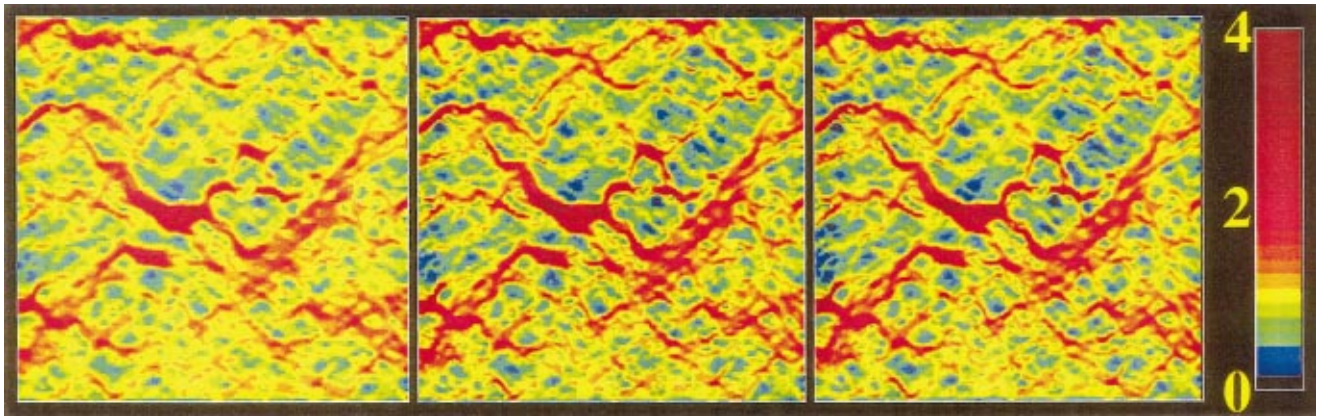

FIG. 1. (Color) The total in-plane momentum flow, normalized to the mean momentum density, in a 32×32 mm^2 portion of the initial fracture at three different spatial resolutions: 250 μm (left), 125 μm (middle), and 62.5 μm (right). The flow direction is from left to right.

controlled erosion, where the local erosion rate depends only on the replenishment of the eroding chemical. It is further assumed that the erosion is slow enough that the velocity field and concentration distribution are time independent at each iteration. To mimic the experimental conditions, where the fracture surfaces were pressed together under a small confining pressure [1], the fracture aperture was closed after each iteration. The surfaces were brought together until the first point of contact and then the upper surface was tilted in the flow direction until a second contact point was reached. A new three-dimensional image of the fracture was then generated and used in the next iteration.

II. METHODOLOGY

Fluid flow in confined geometries, up to Reynolds numbers of about 10, can be described by the Stokes equations for the fluid velocity field $\mathbf{u}(\mathbf{r})$, and pressure $p(\mathbf{r})$ [12]:

$$\nabla\cdot\mathbf{u}=0; \quad \eta\nabla^2\mathbf{u}=\nabla p, \tag{1}$$

where η is the viscosity of the fluid. The Reynolds number, $Re=au/\nu$, characterizing the laboratory experiments of Durham *et al.* [1], can be estimated from the volumetric flow rate (1.3 cm^3/min), the width of the fracture (4.5 cm) and the kinemetic viscosity of water ($\nu=\eta/\rho=0.01$ cm^2/s) to be of order 1. However, even the Stokes equations are difficult to solve in a very irregular geometry, so most simulations of fracture flow assume that the fluid velocity is the same as that between two parallel plates separated by either the mean or the local aperture [13]. However, it has been shown that this approximation has serious shortcomings, especially for small apertures, where it tends to overestimate the permeability [14–16]. In our simulations we have used the much more precise lattice-Boltzmann method [17–19], that has been extensively validated by comparison with experiment, theory and other simulation methods (see Ref. [20] for a recent review). It has been used to simulate fluid flow in a variety of large-scale complex structures, such as porous rocks [21–24] and random configurations of spheres [25–27].

In simulating systems with a changing morphology, repeated calculation of the fluid velocity field is a computational bottleneck, which imposes a severe limitation on the size of systems that can be studied [8]. For example, a conventional lattice-Boltzmann simulation of our fracture topography would require at least five nodes across a typical aperture to get a reasonably accurate velocity field. This means a resolution of about 60 μm for a total of 5×10^6 fluid nodes. In a system of this size it takes about 300 h to compute a single velocity field and thus an erosion simulation of 50 cycles is quite unfeasible. However, a combination of two recent advances in lattice-Boltzmann methodology, outlined below, has brought the computational time down to about 3 h per velocity field, making it possible to study erosion in experimentally relevant samples.

A new boundary condition for the lattice-Boltzmann equation has been developed, in which the solid surface can erode continuously [10,11], thereby minimizing the artifacts introduced by the discrete representation of the fracture surfaces. The accuracy of the new boundary condition is insensitive to the position of the interface with respect to the underlying lattice, and satisfactory results were obtained with 125-μm resolution (see Fig. 1). The reduction in resolution by a factor of 2 over a conventional lattice-Boltzmann simulation of comparable accuracy translates into an order of magnitude saving in computational time and memory. Furthermore, an implicit method has been devised to solve the time-independent equations for low-Reynolds-number (Stokes) flow in porous media [28]. Here, the key idea is to utilize the linearity of the velocity distribution function and solve for the steady-state mass and momentum density directly, rather than allow them to evolve in time. This saves an additional one to two orders of magnitude in computational time. These two ideas combine to give a reduction by at least a factor of 100 in computational time, opening new possibilities for simulation of geophysical flows.

Acid erosion has been modeled by determining the flux of reactant across the boundary surfaces. The concentration field $c(\mathbf{r},t)$, in a time-independent velocity field $\mathbf{u}(\mathbf{r})$, is determined by the convection-diffusion equation,

$$\partial_t c(\mathbf{r},t)+\mathbf{u}(\mathbf{r})\cdot\nabla c(\mathbf{r},t)=D\nabla^2 c(\mathbf{r},t), \tag{2}$$

where D is the diffusion coefficient of the tracer. In this work a stochastic algorithm was used to calculate tracer trajectories that obey the stochastic differential equation

$$d\mathbf{r}(t)=\mathbf{u}(\mathbf{r})dt+\sqrt{2D}d\mathbf{W}(t), \tag{3}$$

where $\mathbf{W}(t)$ is a Gaussian random variable with variance $\langle|\mathbf{W}(t+\Delta t)-\mathbf{W}(t)|^2\rangle=3\Delta t$. The flux of tracer particles across the fracture surfaces can then be determined by particle counting, averaging over an ensemble of tracer trajectories. The flux obtained in this way is equal to the flux obtained from the steady-state solution of the convection-diffusion equation (2) [29]. A tracer diffusion algorithm has a significant advantage over grid-based schemes [8,30–32], in that it can always resolve the diffusive boundary layer that at high Peclet numbers is much smaller than the channel width. In addition, grid-based schemes suffer significantly from numerical diffusion [32], leading to serious errors in the concentration distribution at Peclet numbers that are typical of flow in fractures.

The stochastic algorithm was tested by simulating convection diffusion in a two-dimensional channel of width $W=15$. The fluid was driven by a pressure gradient $\nabla_x p$ between the inlet and the outlet, i.e., $\mathbf{u}(x,y)=(\nabla_x p/2\eta)y(W-y)\hat{e}_x$. Tracer trajectories were calculated with Eq. (3) in the presence of this flow field. A constant and uniform tracer concentration c_0, was imposed at the inlet ($x=0$), and absorbing walls were used at the other boundaries. The flux of tracer particles across the channel walls, $|j_y(x)|=D\partial_y c(x,y)|_{y=0}=-D\partial_y c(x,y)|_{y=W}$, was determined by counting the number of absorbed tracer particles as a function of the distance x from the inlet, averaging over an ensemble of tracer trajectories. The result was compared with boundary layer theory,

$$|j_y(x)|=c_0\overline{u}_x A(\mathrm{Pe})(W/x)^{1/3}, \tag{4}$$

which is valid for high Peclet numbers and positions not too close to the inlet. Here, $\overline{u}_x=W^2\nabla_x p/12\eta$ is the mean flow velocity and

$$A(\mathrm{Pe})=\frac{1}{\Gamma(1/3)}\left(\frac{18}{\mathrm{Pe}^2}\right)^{1/3}, \tag{5}$$

with the Peclet number $\mathrm{Pe}=\overline{u}_x W/D$ and $\Gamma=2.6789\ldots$. Equation (5) is obtained from the convection-diffusion equation (2) by a sequence of steps identical to that taken while calculating solid dissolution into a falling film [33]. For $\mathrm{Pe}>500$, the simulated results agreed with boundary layer calculations to within 5% (see Fig. 2). Here, W and $\overline{u}_x$ were kept constant, while D was varied to modify the Peclet number.

III. RESULTS

We have simulated acid erosion in a fractured specimen of Carrara marble. The topography of the initial fracture surfaces was obtained with a contact profilometer that measured the surface elevation with an accuracy of ± 5 μm on a square grid with a horizontal resolution of 0.25 mm [34]. The total area of each fracture surface was 45×71 mm^2 or 181×286 points. A three-dimensional image of the fracture was reconstructed by replacing the digitized fracture surfaces with an offset from the perfectly mated configuration of 0.50 mm in the longer (flow) direction. The mean aperture, a_0, of the initial fracture was 0.32 mm.

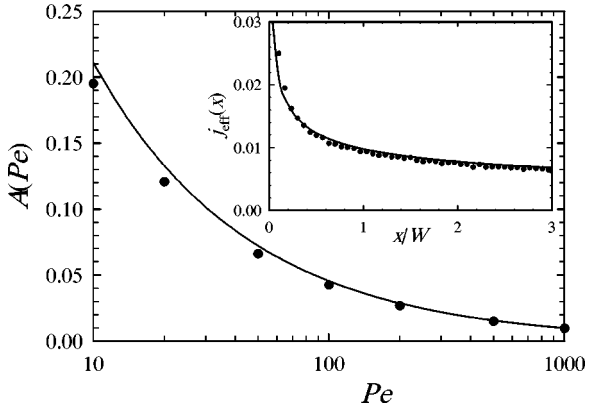

FIG. 2. $A(\mathrm{Pe})$ as a function of the Peclet number. The solid circles are the simulation results and the solid line is the boundary layer theory prediction [Eq. (5)]. The inset shows the reduced flux of tracer particles $j_{\mathrm{eff}}(x)=j(x)/c_0\overline{u}_x$ across the channel walls as a function of the distance from the inlet for $\mathrm{Pe}=1000$.

The effects of grid resolution were evaluated on a 32×32 mm^2 portion of the initial fracture at three spatial resolutions Δ_0/n, with $\Delta_0=0.25$ mm (the lateral resolution of the profilometer) and $n=1$, 2, and 4. The simulated flow field, driven by a constant pressure gradient, was visualized by integrating the steady-state momentum density (normalized to the mean momentum density) over 0.25×0.25 mm^2 columns spanning the entire height of the fracture. The result is shown in Fig. 1 and indicates that the 125-μm resolution already contains most of the details of the flow field. We calculated the root-mean-square velocity fluctuations for the different resolutions and found virtually no

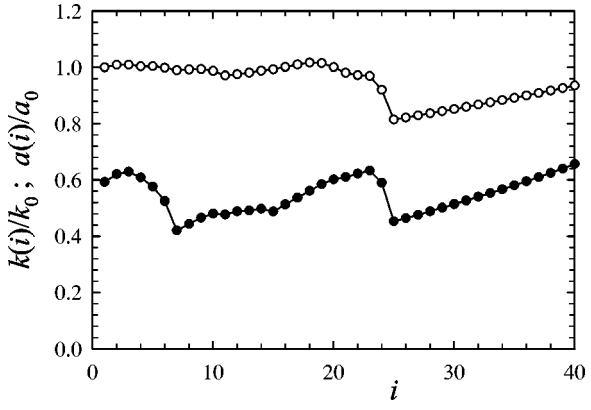

FIG. 3. The permeability $k(i)$ (solid circles) and the mean aperture $a(i)$ (open circles) as a function of the number of iterations i, for a simulation of 40 erosion cycles. The permeability is normalized to the permeability of a straight channel with a height equal to the mean aperture of the initial fracture (a_0), i.e., $k_0=a_0^2/12$.

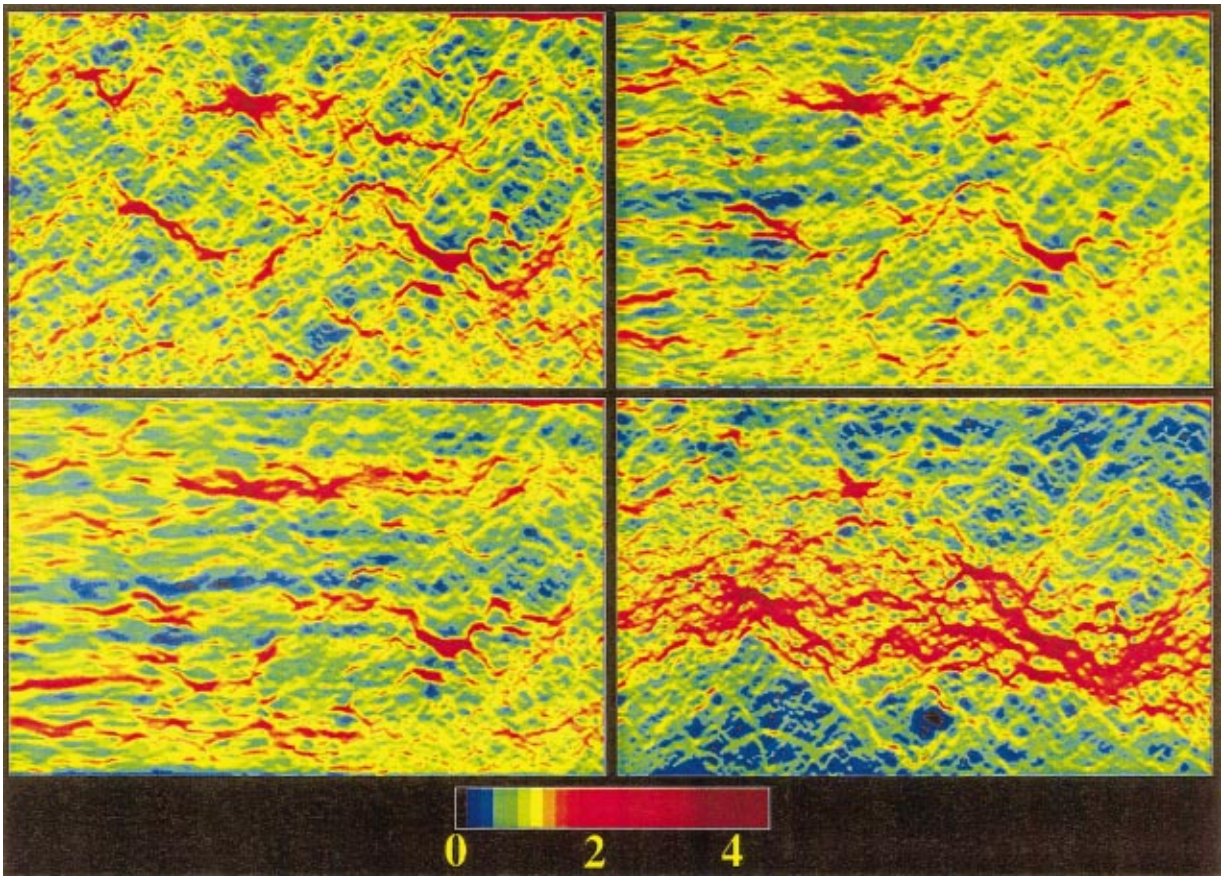

FIG. 4. (Color) The total in-plane momentum flow, normalized to the mean momentum density, at a resolution of 125 μm, in the initial fracture (upper left), after 20 (upper right) and 40 iterations (lower left), and in the experimental fracture after dissolution (lower right). The flow direction is from left to right, the area of each fracture surface was 45×71 mm^2.

difference between the highest two resolutions. Hence, a resolution of 125 μm was used in the erosion simulation. At this resolution the initial size of the full sample was $571\times363\times24$, with a mean aperture of 2.6 lattice spacings and a porosity of about 10%. The initial Peclet number was 270, based on the mean aperture and the mean flow velocity in the fracture. This is comparable to that of the laboratory experiments (Pe$=240$), assuming a reactant diffusion coefficient of 2×10^{-5} cm^2/s.

Tracer trajectories were calculated by solving the stochastic differential equation (3) with a first order method [29]. A constant tracer concentration was imposed at the inlet, and absorbing walls were used at the other boundaries. The time step was chosen such that the largest step size in the initial flow field did not exceed a quarter of a lattice unit. At each iteration the number of tracer particles that crossed the lower and upper surfaces was determined, and an amount of material proportional to the number of hits was eroded from each surface element. The normalization constant was chosen such that the average erosion in the first iteration was 0.025 lattice spacings. New fracture surfaces were created by compressing both surfaces and tilting the upper surface in the flow direction.

Figure 3 shows the permeability $k(i)$ and the mean aperture $a(i)$ as a function of the number of iterations i, for a simulation of 40 erosion cycles. The permeability $k=q_x\nu/\nabla_x p$, is calculated from the mean momentum density in the fracture $q_x=V_f^{-1}\Sigma_{\mathbf{r}\in V_f}\rho u_x(\mathbf{r})$, with ν the kinematic viscosity and V_f the total fluid volume. The permeability is normalized to the permeability of a straight channel with a height equal to the mean aperture of the initial fracture (a_0), i.e., $k_0=a_0^2/12$. The initial decrease in permeability is a result of erosion of contact points near the inlet and the subsequent rotation of the upper surface around a few critical contact points that form a line of pivots roughly (3/5)th of the way down the fracture [see Fig. 4 (top left)]. Although this reduction of the aperture near the inlet has a pronounced effect on the permeability it hardly affects the mean aperture (see Fig. 3), since the decrease of the aperture near the inlet is almost entirely compensated by an increase of the aperture near the outlet. However, gradual erosion of these critical contact points leads to fracture collapse after about 23 iterations and a sudden decrease of both the permeability and the mean aperture.

Figure 4 shows the total in-plane momentum flow (the momentum density integrated over 0.25×0.25 mm^2 columns spanning the entire height of the fracture), normalized to the mean momentum density in the initial fracture (top left) and after erosion of 0.20 cm^3 (top right) and 0.36 cm^3 (bottom left) of material. The morphology of the fracture evolves gradually, from a highly tortuous distribution of

small channels to a much smoother topography with a few main flow channels. The decreased tortuosity is evident in Fig. 4 in the smoothing of the background texture of the sinuous flow channels. It can also be illustrated quantitatively by calculating the change in the ratio of the hydraulic aperture a_h, and the mean aperture [1]. Here, the hydraulic aperture is the height of a straight channel with the same permeability as that of the fracture, i.e., $a_h = \sqrt{12k}$. In Fig. 4, a_h/a increases from an initial value of 0.59 to a final value of 0.75 after 40 iterations, corresponding to a significant overall decrease in tortuosity. At the same time a actually decreased from 2.74 to 2.56 lattice spacings, implying that the decrease in tortuosity was caused by selective erosion of the fracture surfaces, i.e., the formation of relatively straight main flow channels.

The simulated fracture topography after erosion can be compared with that obtained in a laboratory experiment with the same specimen. Durham *et al.* [1] reassembled the initial fracture halves with the same 0.50 mm offset in the flow direction used in the erosion simulation. Care was taken to prevent any sort of lateral movement of the two surfaces once they were brought in contact in this offset configuration. The end faces were sealed to expose only a single narrow slot extending along the full trace of the fracture and to prevent short circuiting of fluid around the rock. Approximately 6.4 l of CO_2-saturated deionized water were passed through the fracture at a rate of 1.3 ml/min until about 0.47 cm^3 of calcite had dissolved. The topography of the fracture surfaces after erosion was obtained with a contact profilometer as described above for the initial fracture surfaces. The flow field derived from the experimental topography after erosion is also shown in Fig. 4 (bottom right).

The experimental topography shows a single large flow channel in the center of the specimen, while the simulation shows a few main channels distributed across the fracture. Furthermore, the simulation exhibited a more pronounced erosion near the inlet than the laboratory experiment. Finally, the ratio of the hydraulic aperture and the mean aperture after erosion was only 0.64 for the experimental topography, compared with 0.75 for the simulated topography. However, the mean apertures after erosion were almost identical (2.56 lattice spacings for the simulated topography versus 2.54 lattice spacings for the experimental topography), indicating a larger reduction of tortuosity in the simulated topography. These discrepancies are most likely a result of the rather crude models for the chemical kinetics and fracture closure.

The current model assumes that all reactants encountering the fracture surfaces cause dissolution. However, even with transport-limited kinetics, the effect of product concentration on the local erosion rate should be included. As material is dissolved the chemical equilibrium is disturbed by the reactants, which slows down further dissolution until these products are convected away. The absence of this mechanism in the simulations leads to excessive dissolution near the inlet. In future work additional tracer particles will be used to represent the product concentration, so that chemical equilibrium between reactants and products can be established. Dissolution can then be modeled by converting reactant tracers to product tracers whenever tracers encounter a solid surface. To account for local chemical equilibrium, the probability of converting a particular reactant tracer to product is dependent on the concentration of reactants and products. Hence, the local erosion rate is limited by convection of products as well as by replenishment of reactants. This improved kinetics model will lead to a more uniform distribution of chemical tracer throughout the fracture and consequently to more uniform erosion in the flow direction.

The effect of the confining pressure on the evolution of the surface morphology may be one of the most important factors, but at the same time is the least understood. For example, it is possible that the presence of a single channel in the experimental data is due to a squeezing of the edges of the fracture by the confining pressure, so that initially straight edges are bowed. This could explain the apparent absence of flow near the boundaries of the fracture. Although the sample was only subjected to a small hydrostatic pressure (0.2 MPa), the contact area is also a small fraction of the total surface area and elastic deformation of the fracture surfaces may not be negligible. Finite element calculations of idealized fractures may give qualitative understanding of the deformation of the contact points and the changes in shape due to an external load. In future work we will examine the sensitivity of the results to some simple assumptions about fracture deformation in order to improve our model of fracture closure. In addition, we intend to investigate the mechanics of the erosion process, and in particular to see if it seems likely that critical support points are being eroded.

IV. CONCLUSIONS

In this paper we have introduced a general method to simulate chemical reactions in porous media on experimentally relevant scales. A typical erosion simulation of 50 cycles takes about 200 h for a fluid volume of 1 cm^3. This makes it possible to begin a systematic study aimed at developing a better understanding of the morphological effects of erosion in porous rocks and the impact that changes in morphology have on the permeability. Preliminary results of acid erosion in a narrow fracture of Carrara marble are reported and compared with experimental measurements. Quite different patterns of erosion are found at large and small length scales, suggesting a strong coupling between transport and morphology. The results are in qualitative agreement with experimental observations, but the quantitative differences indicate that further research is necessary to understand the complex coupling between chemical kinetics, flow, surface morphology, and confining pressure.

ACKNOWLEDGMENTS

We thank Dr. William Durham (Lawrence Livermore National Laboratories) for providing us with the fracture-image data. This work was supported by the US Department of Energy, Chemical Sciences, Geosciences and Biosciences Division, Office of Basic Energy Sciences, and Office of Science Grant No. DE-FG02-98ER14853.

[1] W.B. Durham, W.L. Bourcier, and E.A. Burton, Water Resour. Res. **37**, 1 (2001).
[2] P. Ortoleva, J. Chadam, E. Merino, and A. Sen, Am. J. Sci. **287**, 1008 (1987).
[3] C.I. Steefel and A.C. Lasaga, in *Chemical Modeling of Aqueous Systems II*, edited by D.C. Melchior and R.L. Bassett (American Chemical Society, Washington, DC, 1990), pp. 212–225.
[4] F. Renard, J.-P. Gratier, P. Ortoleva, E. Brosse, and B. Bazin, Geophys. Res. Lett. **25**, 385 (1998).
[5] W. Dreybrodt, Water Resour. Res. **32**, 2923 (1996).
[6] R.B. Hanna and H. Rajaram, Water Resour. Res. **34**, 2843 (1998).
[7] *Proceedings of the Workshop on Initiative for Carbon Management and Climate Change Technology, Gaithersburg, MD, 1998*, edited by W.R. Wawersik and J.W. Rudnicki (Office of Basic Energy Sciences (OBES), Washington, DC, 1998).
[8] S. Békri, J.-F. Thovert, and P.M. Adler, Eng. Geol. (Amsterdam) **48**, 283 (1997).
[9] P. Dijk and B. Berkowitz, Water Resour. Res. **34**, 457 (1998).
[10] R. Verberg and A.J.C. Ladd, Phys. Rev. Lett. **84**, 2148 (2000).
[11] R. Verberg and A.J.C. Ladd, Phys. Rev. E **65**, 016701 (2002).
[12] J. Happel and H. Brenner, in *Prentice-Hall International Series in the Physical and Chemical Engineering Sciences*, edited by N.R. Amundsen (Prentice-Hall, Englewood Cliffs, NJ, 1965).
[13] S.R. Brown, J. Geophys. Res., [Solid Earth Planets] **92**, 1337 (1987).
[14] W.B. Durham and B.P. Bonner, J. Geophys. Res., [Atmos.] **99**, 9391 (1994).
[15] S.R. Brown, H.W. Stockman, and S.J. Reeves, Geophys. Res. Lett. **22**, 2537 (1995).
[16] V.V. Mourzenko, J.-F. Thovert, and P.M. Adler, J. Phys. II **5**, 465 (1995).
[17] G.R. McNamara and G. Zanetti, Phys. Rev. Lett. **61**, 2332 (1988).
[18] F.J. Higuera, S. Succi, and R. Benzi, Europhys. Lett. **9**, 345 (1989).
[19] Y.H. Qian, D. d'Humières, and P. Lallemand, Europhys. Lett. **17**, 479 (1992).
[20] S. Chen and G.D. Doolen, Annu. Rev. Fluid Mech. **30**, 329 (1998).
[21] B. Ferréol and D.H. Rothman, Transp. Porous Media **20**, 3 (1995).
[22] F.M. Auzerais, J. Dunsmuir, B.B. Ferréol, N. Martys, J. Olson, T.S. Ramakrishnan, D.H. Rothman, and L.M. Schwartz, Geophys. Res. Lett. **23**, 705 (1996).
[23] O.v. Genabeek and D.H. Rothman, Annu. Rev. Earth Planet. Sci. **24**, 63 (1996).
[24] W.J. Bosl, Geophys. Res. Lett. **25**, 1475 (1998).
[25] A.W.J. Heijs and C.P. Lowe, Phys. Rev. E **51**, 4346 (1995).
[26] B. Manz, L.F. Gladden, and P.B. Warren, AIChE J. **45**, 1845 (1999).
[27] R.S. Maier, D.M. Kroll, R.S. Bernard, S.E. Howington, J.F. Peters, and H.T. Davis, Phys. Fluids **12**, 2065 (2000).
[28] R. Verberg and A.J.C. Ladd, Phys. Rev. E **60**, 3366 (1999).
[29] H.C. Öttinger, *Stochastic Processes in Polymeric Fluids* (Springer-Verlag, Berlin, 1996).
[30] E.G. Flekkøy, Phys. Rev. E **47**, 4247 (1993).
[31] J.A. Kaandorp, C.P. Lowe, D. Frenkel, and P.M.A. Sloot, Phys. Rev. Lett. **77**, 2328 (1996).
[32] R.G.M.v.d. Sman and M.H. Ernst, J. Comput. Phys. **160**, 766 (2000).
[33] R.B. Bird, W.E. Steward, and E.N. Lightfoot, *Transport Phenomena* (Wiley, New York, 1960), pp. 551–552.
[34] W.B. Durham and B.P. Bonner, Int. J. Rock Mech. Min. Sci. Geomech. Abstr. **30**, 699 (1993).